



Research Article


Preferentially oriented growth of diamond films on silicon with nickel interlayer



Anupam K.C.¹ · Anwar Siddique^{1,4} · Jonathan Anderson¹ · Rony Saha¹ · Chhabindra Gautam² · Anival Ayala¹ · Chris Engdahl³ · Mark W. Holtz^{1,2} · Edwin L. Piner^{1,2} 

Received: 4 August 2021 / Accepted: 22 June 2022

Published online: 15 July 2022

© The Author(s) 2022 

Abstract

A multistep deposition technique is developed to produce highly oriented diamond films by hot filament chemical vapor deposition (HFCVD) on Si (111) substrates. The orientation is produced by use of a thin, 5–20 nm, Ni interlayer. Annealing studies demonstrate diffusion of Ni into Si to form nickel silicides with crystal structure depending on temperature. The HFCVD diamond film with Ni interlayer results in reduced non-diamond carbon, low surface roughness, high diamond crystal quality, and increased texturing relative to growth on bare silicon wafers. X-ray diffraction results show that the diamond film grown with 10 nm Ni interlayer yielded 92.5% of the diamond grains oriented along the (110) crystal planes with ~2.5 μm thickness and large average grain size ~1.45 μm based on scanning electron microscopy. Texture is also observed to develop for ~300 nm thick diamond films with ~89.0% of the grains oriented along the (110) crystal plane direction. These results are significantly better than diamond grown on Si (111) without Ni layer with the same HFCVD conditions. The oriented growth of diamond film on Ni interlayers is explained by a proposed model wherein the nano-diamond seeds becoming oriented relative to the β_1 -Ni₃Si that forms during the diamond nucleation period. The model also explains the silicidation and diamond growth processes.

Article Highlights

- High quality diamond film with minimum surface roughness and ~93% oriented grains along (110) crystallographic direction is grown on Si substrate using a thin 5 to 20 nm nickel layer.
- A detailed report on the formation of different phases of nickel silicide, its stability with different temperature, and its role for diamond film texturing at HFCVD growth condition is presented.
- A diamond growth model on Si substrate with Ni interlayer to grow high quality-oriented diamond film is established.

Relevance Summary This paper describes a method for growing oriented diamond films on silicon substrates using a thin nickel interlayer. The formation of the nickel silicide phase during the early nucleation stage of diamond causes improved columnar growth along the silicide phase. The improved growth mechanism aids in the formation of oriented diamond films with low surface roughness and reduced non-diamond carbon content. Such oriented diamond films with lower non-diamond carbon content have superior optical and thermal properties. Such oriented diamond film growth techniques can be used in GaN-based devices for thermal management applications.

Supplementary Information The online version contains supplementary material available at <https://doi.org/10.1007/s42452-022-05092-y>.

✉ Edwin L. Piner, epiner@txstate.edu | ¹Materials Science, Engineering and Commercialization Program (MSEC), Texas State University, San Marcos, TX 78666, USA. ²Department of Physics, Texas State University, San Marcos, TX 78666, USA. ³Crystallume Inc., 3397 De La Cruz Boulevard, Santa Clara, CA 95054, USA. ⁴Intel Corp., Phoenix, AZ, USA.



Keywords CVD diamond · Oriented growth · Texture · Graphitic co-deposition · Raman spectroscopy · X-ray diffraction

1 Introduction

Superior diamond properties, including a wide band gap, high hardness, chemical inertness, and high thermal conductivity [1–3] make it an attractive material for diverse applications. Diamond films grown by chemical vapor deposition (CVD) are important for thermal management in electronic and optoelectronic devices [4, 5]. Furthermore, the performance of microelectronic devices that operate at high temperature and high-power density would benefit substantially from integration of textured diamond thin films for enhancing heat dissipation [6, 7]. The integration of oriented diamond film in GaN based RF devices can significantly improve the power density and reduce thermal resistivity [5, 6]. For example, GaN-based high-power RF devices fabricated on a diamond substrate showed a $2.7 \times$ reduction in the thermal resistivity, to allow a threefold increase in device areal power density with 85% temperature reduction compared to similar devices fabricated on SiC [8].

Heteroepitaxial growth of diamond films on non-diamond substrates by CVD offers a promising approach for achieving oriented diamond for use in microelectronic applications [9, 10]. The main obstacles to this goal are the high surface energy of diamond, lattice mismatch between the diamond film and substrate as well as intrinsic reactivity of substrate under bias enhanced nucleation compared to other materials [11, 12]. Nickel has a face-centered cubic structure with a lattice constant of 3.52 Å, which differs by only 1.4% with that of diamond (3.57 Å, diamond cubic structure), and has previously been used as a catalytic metal-solvent for high-pressure high-temperature (HP-HT) diamond synthesis [13]. However, graphitic interlayers are generally formed when the Ni substrate is placed in the methane/hydrogen CVD environment [12, 14] and has previously limited the development of an orientational relationship between the diamond film and Ni substrate. Nevertheless, diamond can nucleate and grow on the graphitic layers leading to interesting studies of the high reactivity of carbon in the HP-HT environment and producing new insight into the low-pressure CVD process. Indeed, Sato et al. [15] reported that both (111) and (100) oriented diamond nuclei could be grown on Ni substrates, but the percentage of both nuclei was limited to about 50% and limited details were given with regard to the deposition process. In another study, Hassan et al. [16] reported the formation of high-quality diamond on a WC–Co substrate with Ni interlayer. They annealed the nickel coated WC–Co substrate prior

to diamond growth to enable the nucleation and growth of well-defined diamond crystals, but they did not find oriented diamond nuclei with this approach.

Zhu et al. [12] established a multistep deposition technique for oriented diamond growth on Ni to suppress the graphitic formation by hot filament CVD (HFCVD). They employed a surface pre-treatment multistep annealing process to achieve a consistent orientation of about 85% along either the (100) or (111) directions in a coalesced thick diamond film. Despite these successes, the mechanism by which the oriented nuclei are formed is not fully understood. Furthermore, the high catalytic activity of Ni for hydrocarbon decomposition and high solubility of carbon in Ni often lead to either graphite deposition or no growth if the process is not properly controlled.

A Ni interlayer on Si substrate is different from bulk Ni substrate due to rapid diffusion and high solubility of Ni in Si during thermal processing. This results in the formation of different phases of nickel-silicide [17, 18] beginning at temperatures as low as 200 °C. Epitaxial Ni₂Si starts to form at 200 °C [19]. With increasing temperature, the coexistence of NiSi and NiSi₂ phases is observed in the range 200–650 °C [18, 19]. The silicidation process of Ni on Si substrate and its stability at different temperature has been well established in the literature [20]–[23].

We report for the first time on the improvement of diamond quality and texture with a thin Ni interlayer on Si substrate. A model is proposed in which the formation of silicide phases with diamond growth temperature orients the diamond nuclei along the (110) crystallographic direction with reduced non-diamond carbon phase and minimum surface roughness. The paper is organized in the following structure. The experimental set up, including experimental details and characterization techniques, is presented in Sect. 2. The experimental results are presented in Sect. 3. The results are modeled with a multistep deposition technique to nucleate and grow oriented diamond film on a silicon substrate with a thin intermediate Ni film (less than 20 nm thick) by HFCVD. The extremely high surface energy and lattice misfit between diamond and Si is proposed to be minimized by this process, resulting in a high-quality, highly oriented diamond film on a non-diamond substrate with minimum non-diamond carbon. Furthermore, the oriented growth of diamond nuclei on a non-diamond substrate occurs after 3 h deposition time. In Sect. 4, a summary and the conclusions of this work are presented.

2 Experimental set up

2.1 Experimental details

The samples were prepared by depositing Ni (99.99% purity) of various thickness (nominally, 5, 10, 15, and 20 nm) on 100 mm p-type silicon wafers with (111) orientation in an e-beam deposition system (Angstrom Engineering). The chamber pressure during deposition was 3.63×10^{-8} Torr and Ni deposition rate was 0.5 Å/s. Before diamond seeding, the Ni-coated substrates were sequentially cleaned with acetone, methanol, and isopropanol. Substrates were then seeded with a photolithography process consisting of thoroughly mixed 1 ml dimethyl sulfoxide (DMSO), 3 ml S1813 photoresist, and 1 ml dimethyl sulfoxide (DMSO) based nano diamond suspension (ND) with 0.5 wt.% nano diamond seeds (5–40 nm diameter). Silicon substrates were then spin coated at 2500 rpm speed and 1000 rpm acceleration for 25 s. This blanket seeding method produces a diamond seed density of approximately 10^{10} cm^{-2} [24]. For the diamond HFCVD process, 6 kW was driven through an array of nine tungsten wires, 24 cm long and 0.25 mm diameter, which resulted in a 2200 °C wire filament temperature. The water-cooled rotating substrate was positioned 6 mm from the tungsten wire array to produce a substrate temperature of 720–750 °C as measured by IR pyrometer. Growth was carried out using 30 sccm of methane and 3 sccm of oxygen with 2000 sccm of hydrogen, while maintaining a chamber pressure of 20.8 Torr.

2.2 Sample characterization

The Ni film thickness was measured by spectroscopic ellipsometry (J. A. Woollam Co., Inc.) and X-ray reflectivity (XRR, Rigaku Smart Lab, 3 kW XRD). The surface morphologies of the as deposited Ni films were characterized using atomic force microscopy (AFM, Bruker Dimension ICON). The RMS roughness of the Ni film was found to be < 1 nm with uniform coverage and no Ni spitting was observed. The diamond seeding density on the samples were determined from SEM imaging by using Fiji image J software. For precise seeding density measurement, the S1813 polymer on the seeded wafers were cleaned by etching the polymer using PE50 O₂ Plasma Asher at 100 W power for 3 min in the presence of ionized O₂ gas. After diamond deposition, the surface morphology of the diamond films was characterized by scanning electron microscopy (SEM, FEI Helios 400) and atomic force microscopy. The interface analysis and diamond growth mechanism were studied with cross-sectional

SEM imaging. The cross-section samples were prepared by using standard focused ion beam (FIB) techniques using a Helios Nanolab 400 (Dual beam SEM system) by first depositing a protective Pt layer and milling using a 30 kV accelerating voltage. The composition across the interface was characterized using energy dispersive X-ray spectroscopy (EDS). The quality of the diamond films and the presence of non-diamond carbon phases were characterized by micro-Raman spectroscopy (Horiba LabRAM) equipped with a visible laser (wavelength 532 nm) focused using a 100× objective lens (NA 0.90) for nominal spot diameter ~ 2 μm. Spectra were collected from 450 to 1800 cm⁻¹ for observing the diamond peaks. Low-temperature photoluminescence (PL) measurements [25] (data not shown) were conducted to determine Ni incorporation in diamond using HeCd (325 and 445 nm) laser light for excitation. Emission from nickel color centers was not observed in the reported range, suggesting that any incorporation of Ni is below the PL detection limit in our samples. The oriented diamond film was characterized with XRD (Rigaku SmartLab) leveraging both parallel beam and Bragg Brentano slit configurations operated at 40 kV and 40 mA, with Cu K_α radiation (wavelength 1.5406 Å). Medium resolution $\theta - 2\theta$ XRD scans from 20 to 80° was performed. The diamond film surface roughness was characterized by Dektak XT stylus surface profilometer.

3 Results and discussion

3.1 Characterization of Ni on Si

3.1.1 Ni thickness and roughness

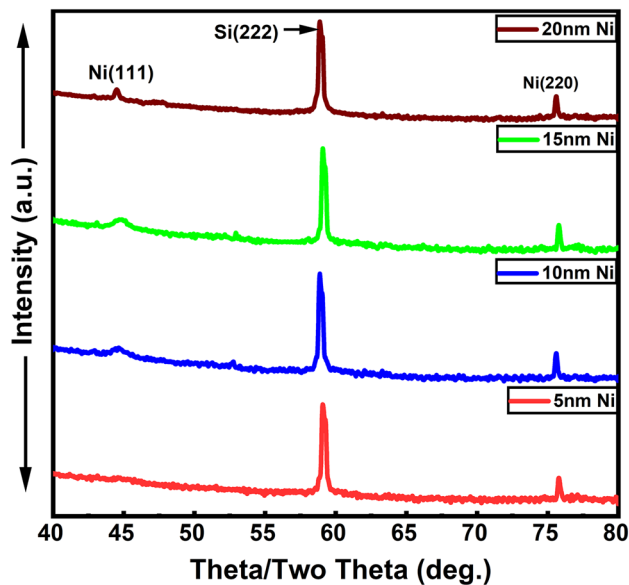
Ellipsometry and XRR results for the as-deposited Ni films on Si (111) are summarized in Table 1. The spectroscopic ellipsometry measurements were taken at two angles of incidence (55° and 65°). The thickness and roughness measured from ellipsometry and XRR generally agree.

3.1.2 XRD analysis for annealed and unannealed Ni film on Si

The crystallographic structure of the Ni layer was evaluated using medium resolution wide-angle parallel beam XRD. Data are shown in Fig. 1. The XRD pattern was compared with standard diffraction peaks given by JCPDS file no.04–0850. We found weak Ni (111) peaks at 44.45° and sharp (220) peaks at 75.30°. The Ni (220) diffraction peak is strongest relative to the Ni (111) peak for the Ni film with 5 nm thickness, which is identified as a highly oriented Ni film along the (220) direction on the Si substrate. From the

Table 1 Thickness and roughness measurements for Ni thin films on Si (111)

Sample	Ellipsometry Results			XRR Results		
	Thickness (nm)	Roughness (nm)	Mean Squared Error (MSE)	Thickness (nm)	Roughness (nm)	R-Squared Value (R^2)
A	4.3 ± 0.3	0.6 ± 0.2	2.3	4.9	0.9	0.01
B	8.8 ± 0.5	0.5 ± 0.2	2.9	8.7	0.3	0.02
C	14.2 ± 0.3	0.3 ± 0.1	3.2	12.8	0.6	0.01
D	16.8 ± 0.3	0.5 ± 0.1	1.9	18.3	0.7	0.03

**Fig. 1** Medium resolution parallel beam XRD scans for Ni thin film on Si

relative intensity ratio, $I(220)/I(111)$, we find progressively higher texturing with thickness with trend 12.4, 9.3, 7.3, and 4.0, respectively for 5, 10, 15, and 20 nm Ni film.

Prior to the diamond growth, the possible phases occurring during the diamond deposition process for Ni layer on Si were identified by conducting a separate study. In this study, 10 nm Ni on Si samples are annealed at two different temperatures, 500 °C and 750 °C, with varying time at low pressure (~ 20 Torr Ar atmosphere) using a tube furnace. The annealing condition, 500 °C for 30 min., is chosen to approximate anticipated silicide formation during the early diamond nucleation period (first 30 min of growth). Results by X-ray reflectivity (XRR) and medium resolution parallel beam XRD are shown in Fig. 2.

For the annealed samples, XRD data in Fig. 2a shows the stable β_1 -Ni₃Si with (002) and (220) crystal orientation at $2\theta = 45.82^\circ$ and 75.89° , respectively, when the samples are annealed for 30 min at 500 °C. The lattice constant calculated from XRD analysis is $a = 3.497 \text{ \AA}$, which is close to the accepted $a = 3.506 \text{ \AA}$ [26] for β_1 -Ni₃Si. Density from

XRR is estimated to be $7.69 \pm 0.81 \text{ g/cm}^3$ in general agreement with the reported β_1 phase of Ni₃Si density 7.9 g/cm^3 [19]. The XRR data are best described using a two-layer model comprised of the silicide and unconsumed nickel. Measurements performed at three different spots on the samples result in an average Ni₃Si phase thickness of $8.2 \pm 1.3 \text{ nm}$ with $3.2 \pm 1.1 \text{ nm}$ Ni on top, see inset Fig. 2b. The thin native silicon oxide layer is no longer observed. We assume this is due to diffusion of O into the Ni during the high temperature anneal [19]. When the annealing temperature is increased to 750 °C for 30 min, strongly textured β_1 -Ni₃Si phase with (220) crystal orientation at $2\theta = 75.89^\circ$ is still present but the surface Ni layer is consumed to form additional silicide (XRD results not shown). The stability of the β_1 -Ni₃Si phase for our samples up to 750 °C for 30 min may be due to the decrease in solubility of Si in Ni for this annealing condition. However, we cannot rule out that the thin (~ 2 nm) native SiO₂ layer plays a role, such as serving as a diffusion barrier, in the silicide formation for our studies. However, the Ni₃Si phase transformed completely into NiSi₂, with a thickness of $14.8 \pm 1.8 \text{ nm}$, when the 750 °C annealing time is increased to 3 h. The formation of NiSi₂ phase is confirmed by the XRD peak at $2\theta = 47.88^\circ$ in Fig. 2a and also by comparing the film density, $4.42 \pm 0.41 \text{ g/cm}^3$, with the standard density [19] based on XRR. Based on this study, it is reasonable to expect the β_1 -Ni₃Si silicide to be present during the early stages of diamond growth and the NiSi₂ phase to form as the deposition process continues.

The (110) texture of the β_1 -Ni₃Si phase after annealing Ni on Si at 750 °C for 30 min is due to the contributions of minimum surface and strain energy present along the {110} grain direction during the silicide formation process. As previously reported, a thin Ni film will develop texture upon annealing and is strongly affected by the deposition conditions and the corresponding driving force for grain growth [27]. The concurrent minimizations of the surface and the strain energies during annealing Ni thin film on Si are identified as the major driving forces for grain growth and the associated texture evolution during silicidation. With increasing annealing temperature, the elastic strain energy dominates over surface energy contributions for

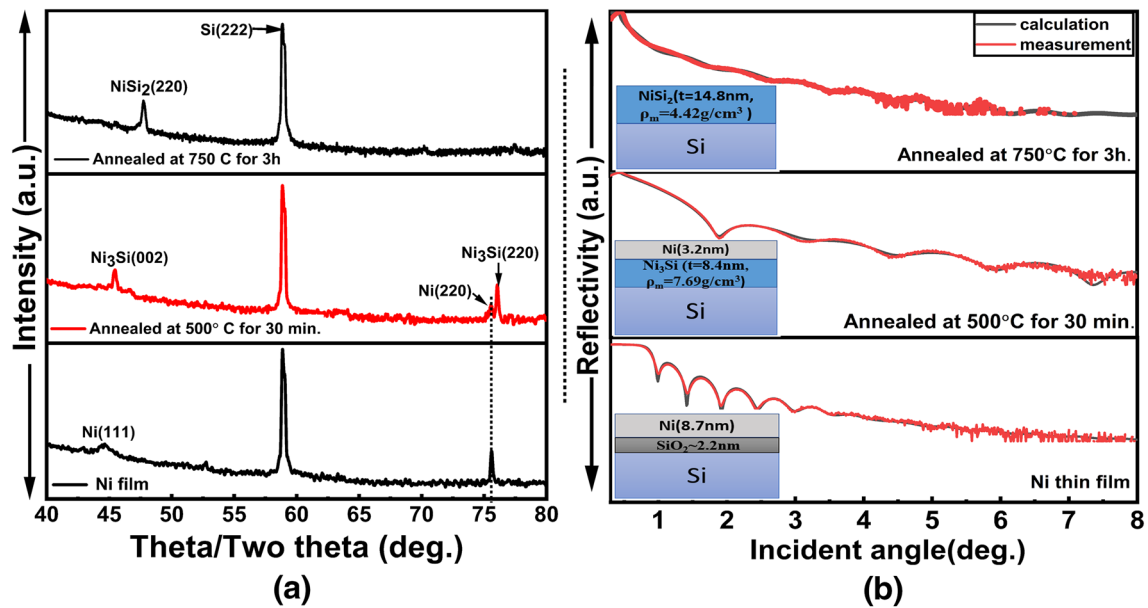


Fig. 2 **a** Medium resolution parallel beam XRD scans for annealed 10 nm Ni thin film at different temperature and time **b** X-ray reflectivity (XRR) scans for the annealed Ni film at different temperature and time

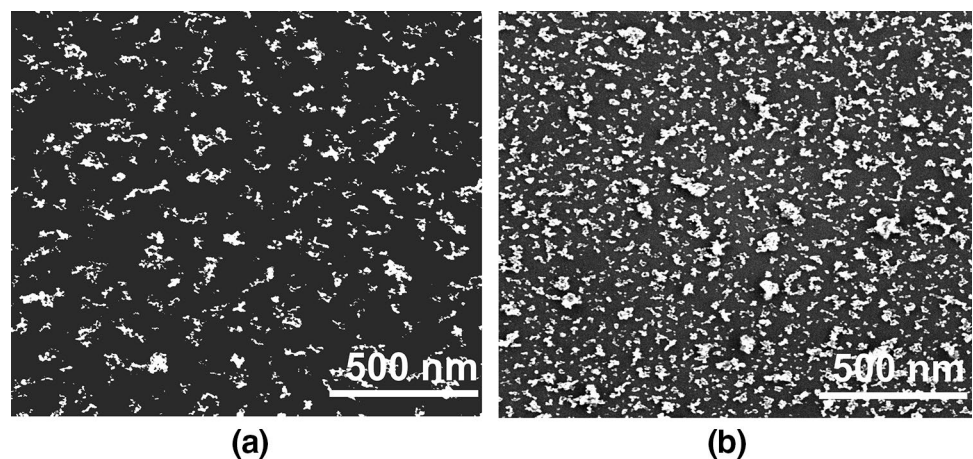
the silicide texture formation [28]. Once the Ni₃Si phase starts to form, the Ni₃Si (110) grains will have lower strain energy thereby yielding anisotropy, as explained by Lu et al. [28]. The resultant sum of surface and strain energy for (110) oriented grains diminish while increasing for (100) and (111) grains. This results in Ni₃Si grains on Si (111) preferably growing along the (110) crystallographic direction giving the strong (220) texture by XRD.

3.2 Characterization of diamond film

3.2.1 Diamond seeding density

The diamond seeding densities on Si (111) and pre-annealed Ni layers are determined from SEM images by using Fiji Image J software. The diamond seeds on the seeded wafers after O₂ plasma etch is shown in Fig. 3. The diamond seeds form an aggregate structure with average aggregate size of (68.20 ± 21.50) nm. The seeds were uniformly distributed across the Ni layer (Fig. 3b) in comparison to the bare Si surface (Fig. 3a). The seeding density calculated by Fiji image J software on the Si and pre-annealed Ni layers was approximately 10^9 cm⁻² and

Fig. 3 SEM images of diamond seeds on **a** Si wafer and **b** Ni layer



10^{10} cm^{-2} , respectively. We obtained 10 times higher diamond seeding density on the Ni layer in comparison to Si. This is due to better adhesion of nano diamond seeds having positive zeta-potential (+35 mV at PH 7) on the Ni surface with negative zeta potential [29] due to enhanced electrostatic interactions including Van der Waals force.

3.2.2 Surface morphology of diamond

SEM images collected after 3 h of diamond growth are shown in Fig. 4 for (a) no Ni interlayer, and (b)–(e) for nominal 5, 10, 15, and 20 nm Ni layers on Si (111), respectively. The diamond thickness is consistent in each sample, 0.32 to 0.38 μm , indicating that nickel does not play a strong role in catalytic growth. In contrast, a significant increase

in diamond grain size is seen with increasing Ni film thickness. The grain size was measured using the Heyn Linear Intercept method [30] from the images, using lines that produced at least 50 intersections. The faceted grain's lateral size ranges from 0.02 to 0.3 μm after 3 h diamond growth. Generally, for diamond deposition, due to different surface structures that depend on crystallography, growth on certain facets will be faster than others leading to a degree of preferential crystal orientation [31]. The diamond nuclei in this study are close to the stable equilibrium shapes, such as octahedral, rhombic dodecahedron, and truncated octahedron, as pictured by the SEM images in Fig. 4. Flake grains due to twin crystals are scarce, and the quality improvement is attributed to the thin nickel layers. Compared to the diamond grown directly on Si

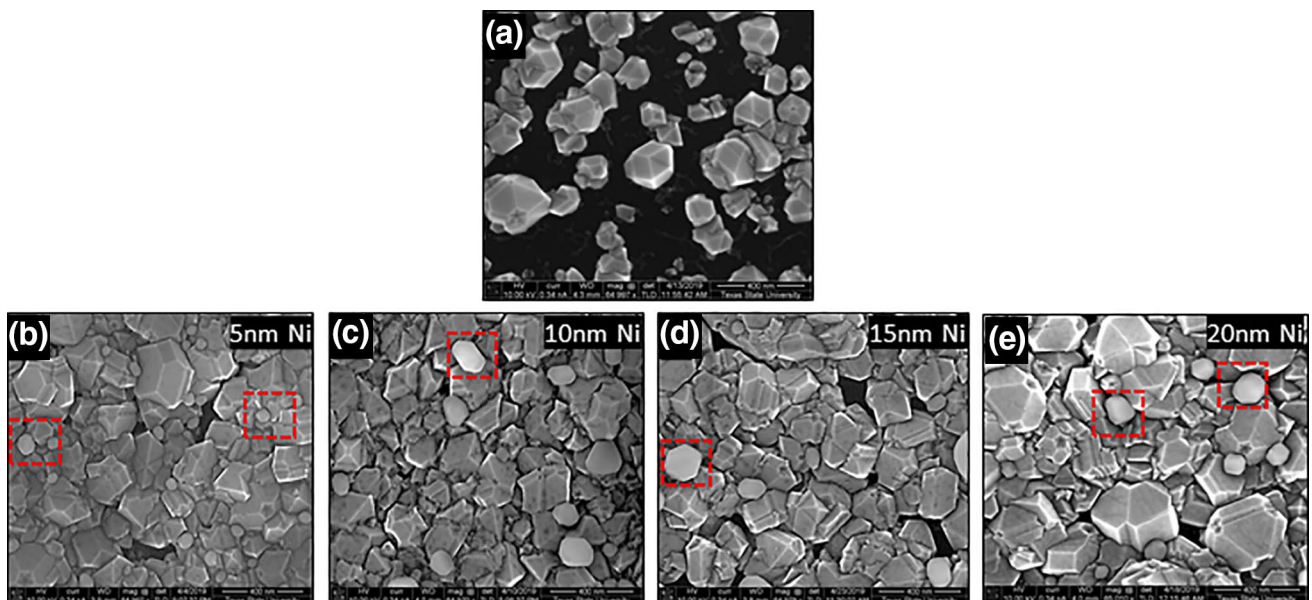
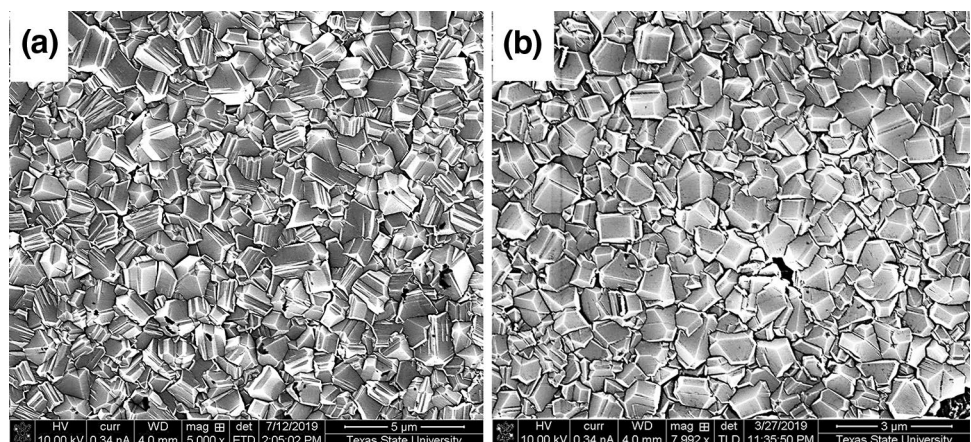


Fig. 4 SEM images of diamond grown for 3 h on **a** Si (111) substrate and **b–e** Ni layers. The red boxes on the images highlight spherically shaped nickel silicide on the diamond surface (characterized by EDS, as shown in Fig. 8b)

Fig. 5 SEM images of diamond grown on **a** 10 nm Ni and **b** Si (without Ni layer) for an additional 6 h (total of 9 h diamond growth)



(111), Fig. 4a, all the diamond films on the Ni layers exhibit substantially better surface coverage and coalescence. This is attributed to better adhesion of the nano diamond to the Ni surface from enhanced electrostatic interaction

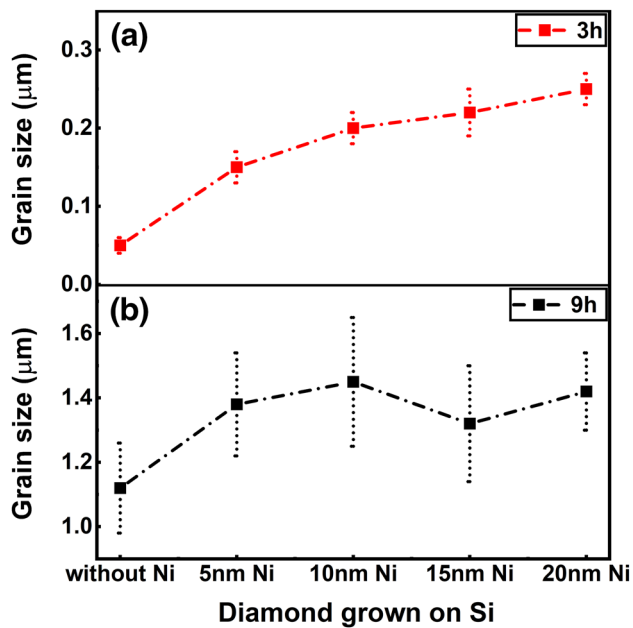


Fig. 6 Average grain size of diamond grown on Si and Ni interlayers after **a** 3 h and **b** 9 h growth

(including Van der Waals forces) [32] leading to higher seeding density, shown in Fig. 3. SEM images are shown in Fig. 5 for diamond on 10 nm Ni and Si substrate (without Ni layer) after an additional 6 h HFCVD. Large-faceted diamond grains have developed on the sample with 10 nm Ni with an average lateral size of $1.45 \pm 0.20 \mu\text{m}$. The increase in lateral grain size is attributed to ripening and takes place in all samples. Average grain size, summarized in Fig. 6a, show the diamond grain size after 3 h growth and Fig. 6b show the grains are substantially larger when diamond is grown with a Ni interlayer after additional 6 h (total 9 h).

Cross-section SEM images for diamond grown with 10 and 20 nm Ni layers are shown in Fig. 7. Thicker nickel silicide is observed at the interface for the 20 nm Ni sample in Fig. 7a compared to the 10 nm Ni sample, shown by Fig. 7b. Unconsumed Ni-Si is also observed on the diamond surface for the 20 nm 3 h Ni sample. The unconsumed Ni-Si present on the diamond surface is seen as round features in the SEM images in Fig. 4. The cross-section SEM images for diamond growth on 10 nm Ni for total 9-h growth is shown in Fig. 7c. This shows that the diamond grain structure after 9 h of growth is fully coalesced and no nickel is observed at the diamond surface.

The nickel silicide phase characterized using EDS is shown in Fig. 8a. The color images indicate the Si substrate, diamond, and nickel appearing in the substrate region. Pt on the sample surface is from the sample preparation

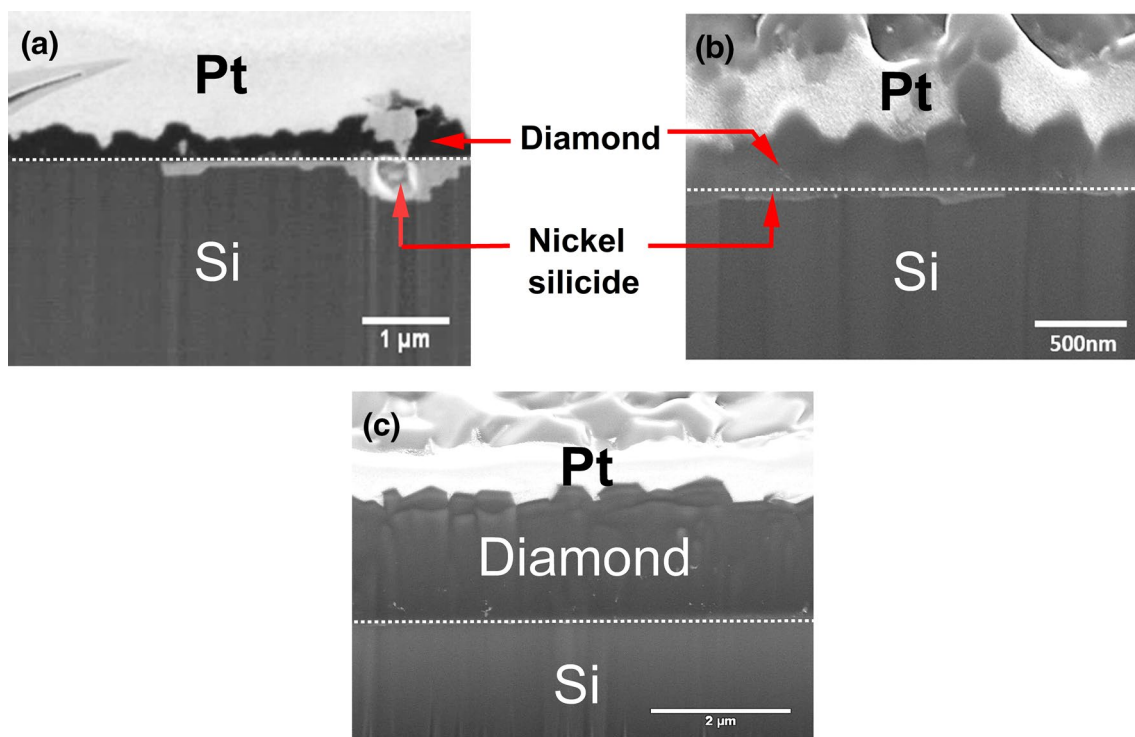
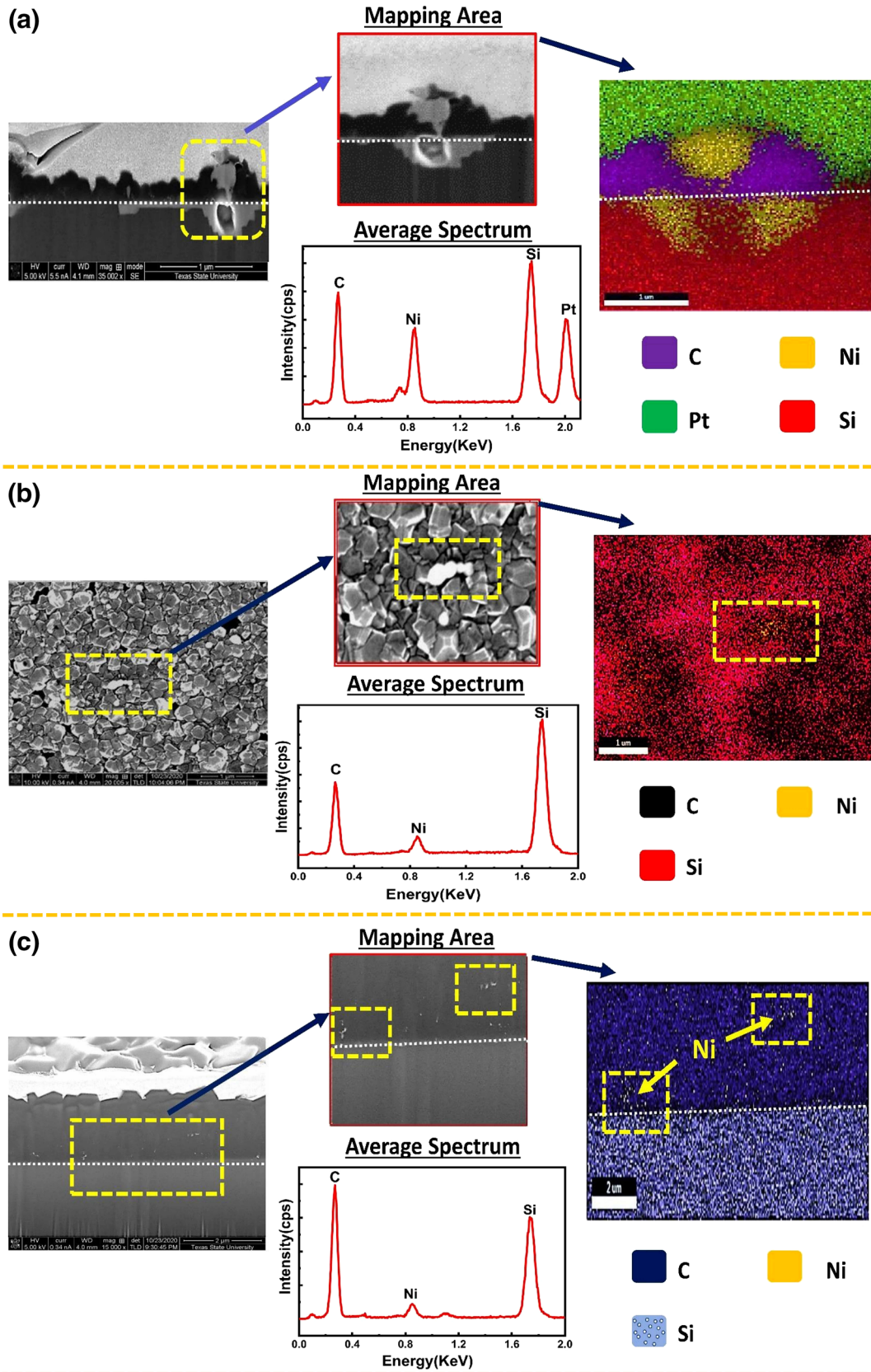


Fig. 7 Cross-section SEM images for diamond grown on **a** 20 nm Ni for 3 h, **b** 10 nm Ni for 3 h and **c** 10 nm Ni for 9 h.



◀**Fig. 8** EDS analysis for **a** the interface phase for the diamond growth on 20 nm Ni for 3 h, **b** the droplets seen on diamond surface after 3 h growth, shown by red boxes in Fig. 4 and **c** the existence of a Ni phase within growing diamond grains for the diamond grown on 10 nm Ni after 9 h

process [33]. The spectrum in Fig. 8a gives the relative EDS peak intensities of the indicated elements.

The EDS analysis for the composition of the rounded features on the diamond surface, Fig. 4, is observed to be an intermediate Ni, C, and Si phase and shown in Fig. 8b. The size of these features is smaller for diamond grown on the thin Ni layer and increases in size with increasing Ni thickness for the investigated growth time of 3 h. The appearance of Ni, C, and Si rounded feature on the diamond surface after 3 h diamond growth confirms that the Ni interlayer plays a role in both silicide formation, seen in Fig. 4a, and diamond nucleation. Above this thickness, additional diamond growth may result in Ni residing at the growth surface and possibly within the diamond. Traces of Ni in the boundaries between the diamond grains is observed from the EDS mapping at the interface for diamond grown on 10 nm Ni for an additional 6 h (total 9 h) is shown in Fig. 8c. This result is interpreted as evidence that the nickel droplets present after 3 h diamond growth decay into smaller droplets at the diamond growth temperature of $\sim 750^\circ\text{C}$ for longer growth time.

3.2.3 Quality of diamond film

3.2.3.1 Raman spectroscopy Visible Raman analysis was performed to investigate the diamond crystallinity development after 3 h growth. The results for each sample are shown in Fig. 9a. The diamond O (Γ) phonon peak is centered at 1332 cm^{-1} . The broad Raman features at 1363 cm^{-1} and 1567 cm^{-1} correspond to the D and G bands of disordered carbon, respectively. The peaks at 1139 cm^{-1} and around 1492 cm^{-1} are related to trans-polyacetylene (t-PA) at grain boundaries and surfaces, characteristic of nanocrystalline diamond [32]. The disordered carbon and nanocrystalline diamond features are slightly more pronounced in the samples grown with a Ni interlayer. Raman spectra are shown in Fig. 9b for the thick diamond films grown for the additional 6 h (total 9 h) HFCVD process. In all cases the diamond O (Γ) dominates the spectra, and when grown directly on Si we also see the disorder and nanocrystalline features. In contrast, spectra for samples grown with the Ni interlayer exhibit weak D and G bands, and very weak scatter associated with nanocrystalline diamond. The following important trends can be concluded from the Raman spectra: (1) diamond grown both directly on the Si substrate and the Ni layers exhibits similar carbon related Raman signals, (2) the enhanced nucleation of

diamond film on Ni layers have suppressed non-diamond peaks when growing thicker diamond layers. These results indicate that the presence of the thin Ni film improves the HFCVD diamond quality.

Trends in the diamond volume fraction are obtained by calculating the ratio of integrated intensities (area under the curve after background correction) of diamond peak, I_D , to the total intensity from diamond plus that from the non-diamond carbon, I_{NDC} [34, 35]. This is expressed as $I_D/(I_D + I_{NDC})$. The observed trend in Fig. 10, for 9 h total HFCVD diamond growth, shows improved diamond intensity ratio for diamond grown with Ni layers compared to diamond grown on Si without Ni. This result is consistent with nickel assisting with the conversion of non-diamond carbon into diamond during growth. The FWHM of the diamond O (Γ) Raman line, shown in Fig. 10, exhibits a reduction, corresponding to improved material, for the thinnest Ni interlayers. The improvement in diamond film quality with Ni interlayer is a result of slightly faster diamond nucleation/growth kinetics on Ni layers. The fast diamond coalescence on Ni layers results in decreased NDC content. Thus, the Ni layer improves the diamond crystalline quality by reducing the non-diamond carbon concentration.

3.2.3.2 Surface roughness and thickness The thickness and root-mean-square (RMS) roughness of the diamond film are characterized by cross-section SEM and profilometer, respectively, and shown in Fig. 11. The diamond surface roughness for 9 h growth on Ni layer is lower in comparison to the diamond film grown directly on Si, while the diamond film thickness is $\sim 2.5\ \mu\text{m}$. The lower diamond film surface roughness is a result of fast coalescence of diamond on Ni. The increased surface roughness for the thicker films after 9 h growth in comparison to 3 h growth is attributed to the larger grain size. Diamond growth rate depends on the growth temperature [36]. During nucleation (within the 1st hour of growth), the temperature of the system rises slowly to reach $\sim 750^\circ\text{C}$ and the incubation time between diamond nucleation from graphitic layers to convert sp^3 bonded carbon is relatively longer. Once the growth is stabilized at $\sim 750^\circ\text{C}$, the available carbon may convert to sp^3 (diamond) and the growth rate correspondingly increases. This process explains how the diamond growth rate during the first 3 h is $\sim 0.1\ \mu\text{m}/\text{h}$ while averaging $\sim 0.3\ \mu\text{m}/\text{h}$ over 9 h of growth.

3.2.4 Diamond texture analysis by XRD

The diamond film texture characterized by medium-resolution wide-angle parallel beam XRD, is shown in Fig. 12, for 3 h diamond growth. The XRD scans reveal sharp (220) diamond peaks at 75.6° and weak (111) peaks at 43.9° . The (220) NiSi_2 peak at 47.8° is due to the precipitated

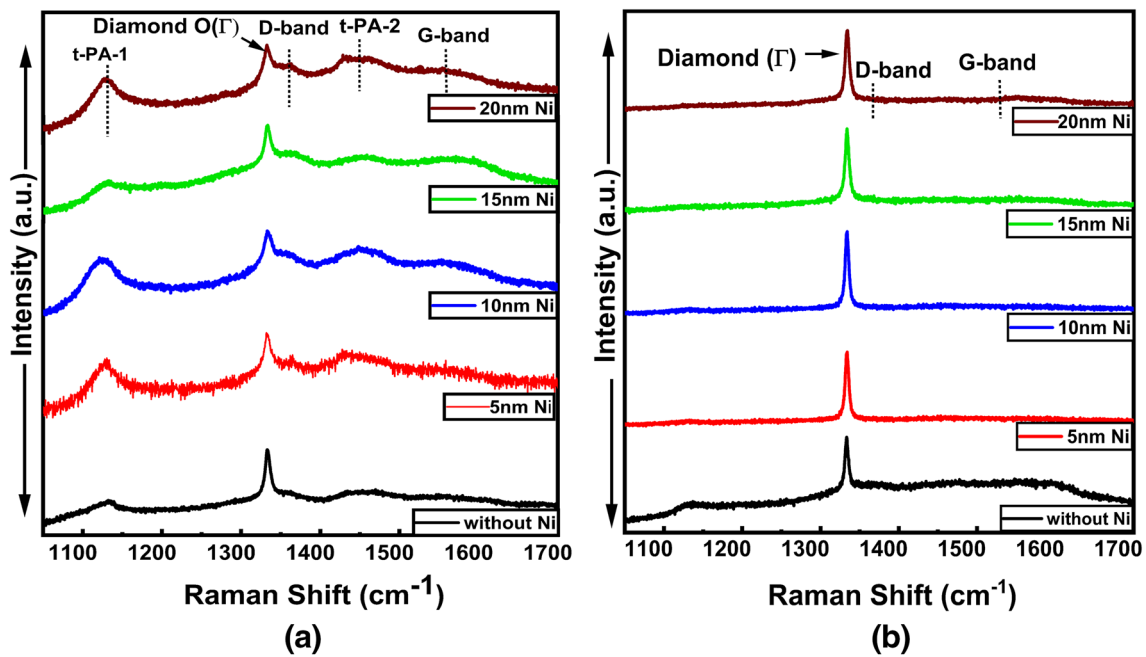


Fig. 9 Raman spectra for diamond grown on Ni layer with different thicknesses for **a** 3 h and **b** 9 h (3 h + 6 h)

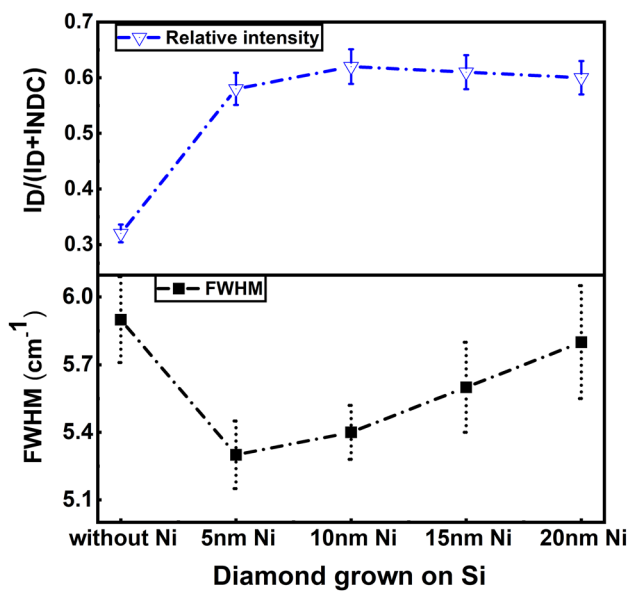


Fig. 10 Relative peak intensity (I_D/I_{D+INDC}) and diamond peak FWHM of 9 h HFCVD grown diamond with Ni layer thickness

silicide phase at the diamond surface and at the interface during diamond growth (shown in SEM images, Fig. 4, Fig. 7a). Ni_3C with (111) and (200) crystallographic peaks at 44.6° and 51.9° are seen for the diamond film grown with 20 nm Ni. This phase has rhombohedral crystal structure at diamond growth temperature $\sim 750^\circ C$ with nearly 9.5 at. % of C [37]. To quantify the diamond film texture, the

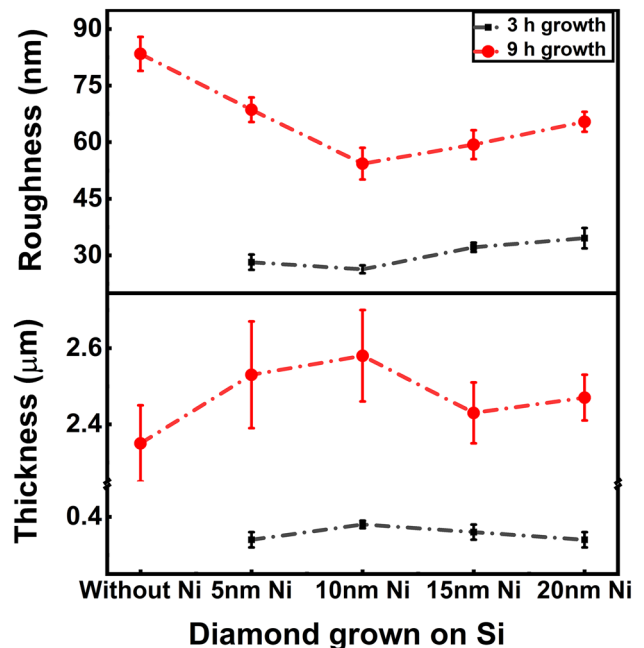


Fig. 11 Thickness and roughness of diamond film grown for different times

observed intensities were compared to the spectrum from a randomly oriented diamond powder sample. The planar indices, 2-theta angle, d -spacing and expected random intensities of the diffracted beam for a randomly oriented diamond powder were taken from the American Society

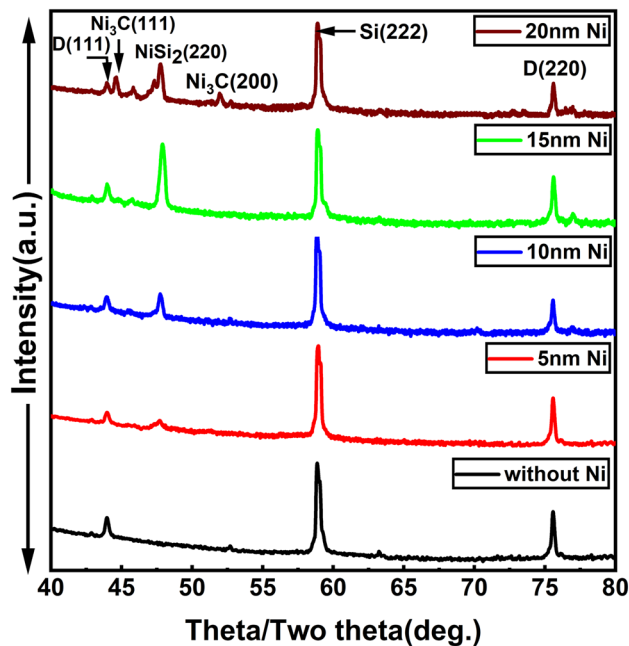


Fig. 12 Medium resolution parallel beam XRD scans for diamond films grown on the varying Ni layer thickness for 3 h

Table 2 The relative intensity of diffracted X-rays beams for random assembly of diamond crystals [38]

h, k, l planer indices	2 θ angle(degree)	d-spacing (Angstrom)	Relative diffracted intensity
(111)	43.9	2.06	100
(220)	75.6	1.261	25
(311)	91.5	1.0754	16
(400)	119.5	0.8916	8
(331)	140.3	0.8182	16

of Testing Materials (*ASTM Card info 6–0675*) and are given in Table 2.

The observed peak intensities for the diamond 2 θ peaks (43.9° and 75.6° for diamond (111) and (220), respectively) are calculated for all samples utilizing the Lorentzian curve fitting technique. The integrated peak intensity (I_{hkl}) of the respective peaks is determined by multiplying the observed peak intensity by the peak's FWHM. Each measured integrated peak intensity is divided by the relative diffracted intensity from the randomly oriented powder. Finally, the values are expressed as a percentage peak intensity according to

$$(220) \text{ Texture } (\%) = \frac{\frac{I(220)}{25}}{\left(\frac{I(220)}{25} + \frac{I(111)}{100}\right)} \times 100 \quad (1)$$

where $I(220)$ and $I(111)$ are the integrated peak intensities of the (220) and (111) peaks, respectively. The calculated texture values are expressed graphically in Fig. 13a. From the analysis, the diamond films grown with Ni interlayer are substantially more textured toward (110) compared to diamond grown directly on silicon. For 3 h growth, the 10 nm Ni layer has marginally higher (110) oriented diamond compared to the other Ni film thicknesses, as well as the lowest surface roughness (Fig. 11). Finally, the diamond texture is analyzed following an additional 6 h (total 9 h) diamond growth comparing without Ni layer and with 10 nm Ni layer. Without Ni, the percent texture values do not change significantly from those found following 3 h growth. However, increased (110) texturing is observed for the 10 nm Ni layer sample. The high nucleation kinetics of diamond enables additional (110) texturing, to 92.5%, on the 10 nm Ni layer sample upon further diamond growth with ~2.5 μm thickness. This result shows significantly enhanced texturing compared to diamond grown directly on Si for the same growth conditions and comparable thicknesses.

3.2.5 Discussion

The growth of highly oriented diamond films can be explained by the nano-diamond seeds orienting within the $\beta_1\text{-Ni}_3\text{Si}$ phase during the early diamond nucleation period. We found (110) preferential crystal orientation of $\beta_1\text{-Ni}_3\text{Si}$ on Si during the diamond nucleation period by separate experiments on annealed Ni films on Si discussed in Sect. 3.1.2. $\beta_1\text{-Ni}_3\text{Si}$ has the $L1_2$ -type crystal structure (ordered face cubic structure, 221 space group) with Si and Ni located at 1a and 3c Wyckoff positions [22], respectively, as illustrated in Fig. 14a, along with the diamond structure in Fig. 14b. The unit cell lattice parameter is 3.506 Å [23], and is ~1.7% lattice mismatched with diamond (at room temperature). In addition, the (220) peaks position for diamond ($2\theta = 75.60^\circ$) and $\beta_1\text{-Ni}_3\text{Si}$ ($2\theta = 75.89^\circ$) indicates a mismatch of 0.4% along this crystallographic plane. So, an epitaxial relationship between diamond and $\beta_1\text{-Ni}_3\text{Si}$ phase is expected.

We now describe a proposed model for the diamond formation with texturing caused by the presence of the nickel silicide. During nucleation, the diamond seeds embed in the eutectic $\beta_1\text{-Ni}_3\text{Si}$ phase, possibly residing mostly at the grain boundaries. The diamond seeds will, thus, preferentially orient along the (110) direction and start to grow with orientation subject to the predominant

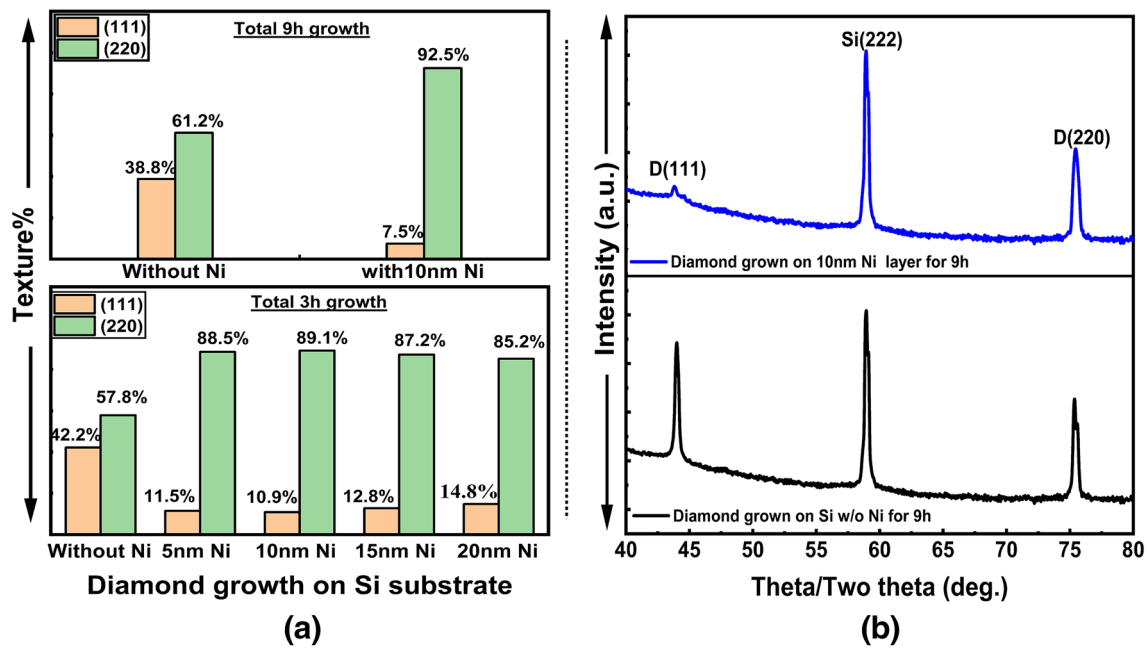


Fig. 13 (a) Crystal orientation distribution of diamond obtained from XRD for the samples grown with varied Ni layer thickness. (b) Medium resolution parallel beam XRD scans for diamond grown on Si and 10 nm Ni layer for an additional 6 h (total 9 h)

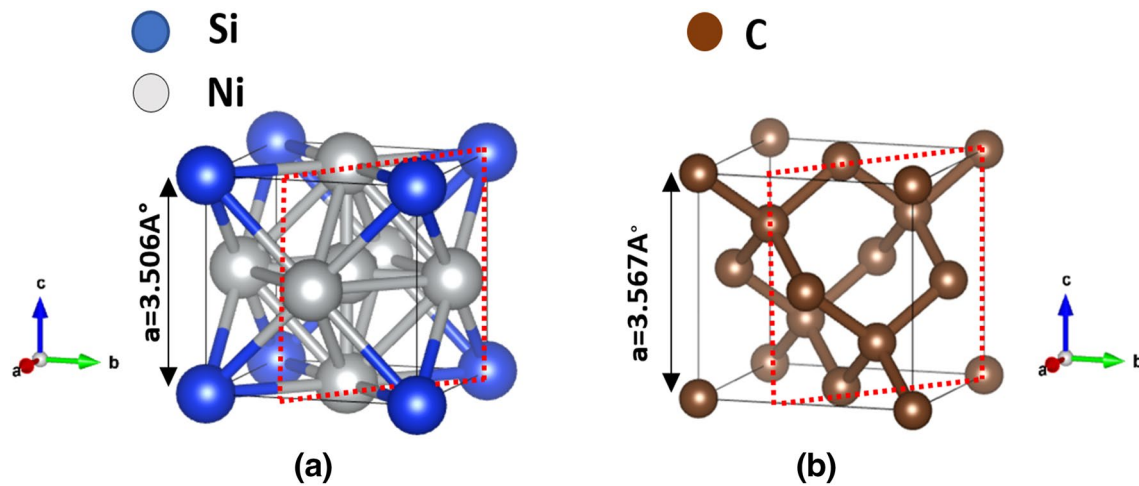


Fig. 14 Representation of (220) crystal plane (red dashed rectangles) in crystal structures for **a** β_1 -Ni₃Si and **b** Diamond

β_1 -Ni₃Si crystal facet. The carbon and hydrogen that remain on the surface provide an additional pathway for diamond deposition resulting in a diamond film textured along the (110) direction. This is an important difference between our results and other published literature results [39, 40]. Previous studies used different multi-deposition processes that produced oriented diamond only after several microns (15–20 μm) of diamond growth. In contrast, we have obtained (110) preferentially oriented diamond within the first 300 nm of diamond film thickness, along with further texturing with thicker ($\sim 2.5 \mu\text{m}$) diamond

film. In all cases, substantially higher diamond texture is observed in comparison to diamond grown directly on Si.

3.2.6 Diamond growth model on Ni thin film

We now propose a model for seeded diamond growth on silicon with nickel interlayer as depicted in Fig. 15a–h. It has been reported by others that when diamond is grown on a thick nickel substrate, a graphitic carbon layer is observed to form under HFCVD conditions [12]. It is reasonable to consider that a similar layer may form in the

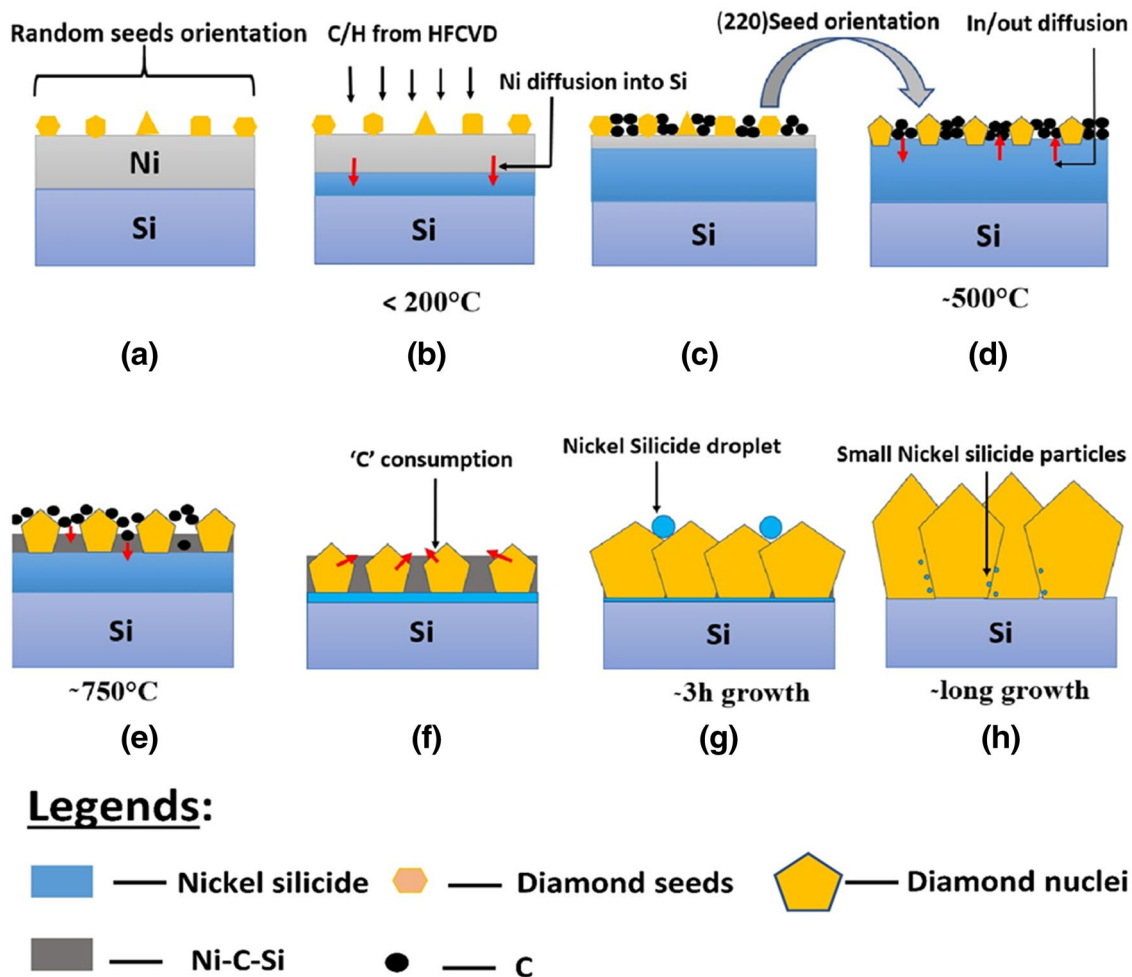


Fig. 15 Schematic representation of diamond growth model on Ni thin film on Si substrate

early growth stages for our thin film Ni samples. However, a key difference in our studies is that when the temperature exceeds 200°C , the Ni begins to diffuse into the silicon substrate and a nickel silicide phase is initiated [20]. The interdiffusion is expected to increase as the temperature increases. As discussed above, when annealing at 500°C the silicide was found to form in the $\beta_1\text{-Ni}_3\text{Si}$ phase as confirmed by XRD in Fig. 2a. The formation of nickel silicide phase can also be seen for our samples in cross-sectional SEM images shown in Fig. 7a, b, which is also characterized by EDS and shown in Fig. 8a. The diamond seeds present on the top surface embed in the $\beta_1\text{-Ni}_3\text{Si}$ phase. Since $\beta_1\text{-Ni}_3\text{Si}$ and diamond have comparable lattice parameters, the diamond seeds may attach to and possibly orient with the silicide surface, modeled in Figs. 15c, d. The supply of C and H from the HFCVD process produce the anticipated diamond growth to the seeds that tend to orient according

to the presence of the silicide. This modifies the diamond columnar growth mechanism and texture.

The Ni-C-Si material may form due to high reactivity of Ni in C, to form a Ni-C phase, and Si atoms reacting with C. Such a process is likely to be starved of Ni and Si as the former is incorporated into the silicide and supply of the latter from the substrate diminishes with diamond thickness. The evidence of the formation of a Ni, C, and Si intermediate phase on the growing diamond surface is supported by EDS data for the samples shown in Fig. 8b. Once Ni-C-Si is formed and the temperature continues to rise, the C solubility decreases and begins to separate out from the silicide. Then, the separated C atoms act as another carbon source, which is consumed by the growing diamond nuclei to form larger diamond grains. The formation of large diamond grains for the diamond grown on Ni layer for 3 h and additional 6 h (total 9 h) on our samples is shown in Fig. 6. We speculate that once the C is consumed from Ni-C-Si

phase, the remaining Ni-Si phase precipitate out as spherical droplets [41] on the diamond surface ($\sim 725^\circ\text{C}$) and then solidify on the diamond surface during cooling. The precipitate's rounded shape droplet is only observed when the diamond growth is limited to a short period (3 h). The nickel silicide precipitates formed on the diamond surface after 3 h diamond growth is seen in the SEM images in Fig. 4, and which is characterized by EDS and shown in Fig. 8b. Upon subsequent diamond growth, these droplets slowly dissolve with a few remaining in the diamond grain boundaries. Traces of Ni that appear on the growing diamond surface on our samples after growing an additional 6 h (total 9 h) of diamond on 10 nm Ni are shown in Fig. 8c. The resultant diamond film will have highly oriented grains along with silicide phase during diamond nucleation with improved quality. The (110) oriented diamond film on our samples along with the $\beta_1\text{-Ni}_3\text{Si}$ phase can be seen by quantitative x-ray diffraction analysis shown in Fig. 13a. Similarly, their improved quality can be seen from the Raman spectroscopy analysis shown in Fig. 10.

The stepwise model for diamond growth on a thin nickel interlayer on silicon is shown in Fig. 15 and explained as follows:

- a. Fig. 15a represents the nano-diamond seeded wafer. When heated in the HFCVD chamber, Ni begins diffusing into the Si. When the HFCVD temperature is below 200°C , C and H radicals also start to diffuse into the top Ni layer, as shown in Fig. 15b.
- b. With increasing growth temperature, above 200°C , the Ni diffusion rate into the Si increases and complete transformation into the silicide phase occurs, as shown in Fig. 15c. The C and H radicals from the HFCVD growth environment diffuse into the silicide phase and may also act as source material for nano-diamond seeds for growth into larger grains.
- c. The diamond seeds embed into the silicide phase and possibly start to orient along the silicide's crystallographic direction. These oriented seeds act as the preferred nucleation sites to grow into larger grains with the incoming C radicals. At $\sim 500^\circ\text{C}$, C and H would be diffusing into the Ni-Si phase to form Ni-Si-C intermediate phases, as shown in Fig. 15d.
- d. Above 500°C , the Ni-C-Si phases continue to form. With increasing growth temperature, the C solubility decreases and would be expected to separate out from the Ni-Si phases. The out-diffusing C can act as an additional source for the growth of diamond, by being incorporated into the growing diamond nuclei. These steps are shown in Fig. 15e, f.
- e. At the diamond growth temperature of $\sim 750^\circ\text{C}$, the Ni-Si phase may precipitate out as droplets after all C is

consumed from the Ni-Si-C phase. The droplets solidify during cooling and can be seen on the diamond surface after 3 h growth time, as shown in Fig. 15g. During further HFCVD diamond growth, these droplets slowly dissolve and may incorporate along the diamond grain boundaries, as represented in Fig. 15h.

4 Conclusions

Growth of diamond on silicon with thin Ni interlayers yields increased diamond nucleation density resulting in the formation of highly textured, coalesced diamond films after 300 nm diamond deposition by HFCVD. The highly textured diamond films orient along the (110) crystallographic direction within 3 h growth time. Further diamond texturing, up to 92.5%, is observed following an additional 6 h growth, yielding an $\sim 2.5\ \mu\text{m}$ thick diamond film. The best results are obtained with a 10 nm thick Ni layer that produces the optimal nickel-silicide thickness for orienting the diamond nano-seed. The resultant diamond film has lower surface roughness and less non-diamond carbon (NDC) in comparison to the diamond film grown on Si without the Ni layer, with comparable diamond film thickness. We propose that the improved orientation observed in the diamond film is due to improved columnar growth within the $\beta_1\text{-Ni}_3\text{Si}$ that forms as Ni diffuses into the silicon wafer during the early nucleation step. Using a thin Ni interlayer ($< 20\ \text{nm}$) on Si to achieve preferentially oriented diamond film is applicable for thermal management in various microelectronic applications. Integration of oriented diamond film on Si as a substrate with technological materials, such as GaN based high electron mobility transistors, will reduce the thermal boundary resistance, and take advantage of the benefits of diamond heat conduction away from the device active region.

Authors' contributions Anupam K.C.: Principal researcher, writing original draft preparation. Anwar Siddique: Initial diamond research. Jonathan Anderson: Microscopy characterization. Rony Saha: XRD characterization. Chhabindra Gautam: Sample preparation and growth. Anival Ayala: Diamond growth. Chris Engdahl: Supervision, hardware. Mark W. Holtz: Supervision, Raman, Writing- Reviewing and Editing. Edwin L. Piner: Overall supervision, Writing- Reviewing and Editing.

Funding Funding for this work was provided by the National Science Foundation (ECCS 1810419) under the direction of Dr. Dimitris Pavlidis.

Availability of data and material The data/materials may be available upon requesting to corresponding author. Code availability Not applicable.

Declaration

Conflict of interest The authors declare that they have no competing interests.

Consent to participate Not applicable.

Consent for publication Not applicable.

Ethics approval Not applicable.

Open Access This article is licensed under a Creative Commons Attribution 4.0 International License, which permits use, sharing, adaptation, distribution and reproduction in any medium or format, as long as you give appropriate credit to the original author(s) and the source, provide a link to the Creative Commons licence, and indicate if changes were made. The images or other third party material in this article are included in the article's Creative Commons licence, unless indicated otherwise in a credit line to the material. If material is not included in the article's Creative Commons licence and your intended use is not permitted by statutory regulation or exceeds the permitted use, you will need to obtain permission directly from the copyright holder. To view a copy of this licence, visit <http://creativecommons.org/licenses/by/4.0/>.

Appendix A. Supplementary data

Results for diamond grown on 10 nm Ni layer without diamond seeding and other supporting data is provided as a supplementary file.

References

1. Kim M, Seo JH, Singiseti U, Ma Z (2017) Recent advances in free-standing single crystalline wide band-gap semiconductors and their applications: GaN, SiC, ZnO, β -Ga₂O₃, and diamond. *J Mater Chem C* 5(33):8338–8354. <https://doi.org/10.1039/c7tc02221b>
2. Faili F, Palmer N, Oh S, Twitchen D (2017) Physical and thermal characterization of CVD diamond: a bottoms-up review. In: 16th IEEE intersociety conference on thermal and thermomechanical phenomena in electronic systems (ITherm), pp 79–86. <https://doi.org/10.1109/ITHERM.2017.8023958>
3. Huang Q, Yu D, Xu B, Hu W, Ma Y, Wang Y, Zhao Z, Wen B, He J, Liu Z, Tian Y (2014) Nanotwinned diamond with unprecedented hardness and stability. *Nature* 510(7504):250–253. <https://doi.org/10.1038/nature13381>
4. Lu YJ, Lin CN, Shan CX (2018) Optoelectronic diamond: growth, properties, and photodetection applications. *Adv Opt Mater* 6(20):1–16. <https://doi.org/10.1002/adom.201800359>
5. Gerrer T, Yu D, Xu B, Hu W, Ma Y, Wang Y, Zhao Z, Wen B, He J, Liu Z, Tian Y (2018) Transfer of AlGaIn/GaN RF-devices onto diamond substrates via van der Waals bonding. *Int J Microw Wirel Technol*. <https://doi.org/10.1017/S1759078718000582>
6. Ahmed R, Siddique A, Anderson J, Gautam C, Holtz M, Piner E (2020) Integration of GaN and diamond using epitaxial lateral overgrowth. *ACS Appl Mater Interfaces* 12(35):39397–39404. <https://doi.org/10.1021/acsami.0c10065>
7. Guo F, Li T, Man H, Liu K, Wang X (2021) Enhanced heat dissipation of GaN RF devices based on double-diamond structure. In: 2021 6th international conference on integrated circuits and microsystems (ICICM), pp 55–60. <https://doi.org/10.1109/ICICM54364.2021.9660259>
8. Altman D, Tyhach M, McClymonds J, Kim S, Graham S, Cho J, Goodson K, Francis D, Faili F, Ejeckam F, Berstein S (2014) Analysis and characterization of thermal transport in GaN HEMTs on Diamond substrates. In: Thermomechanical phenomena in electronic systems -proceedings of the intersociety conference, pp 1199–1205. <https://doi.org/10.1109/ITHERM.2014.6892416>
9. Linnik SA, Zenkin SP, Gaydaychuk AV (2021) Heteroepitaxial diamond growth from the gas phase: problems and prospects (review). *Instrum Exp Tech* 64(2):177–189. <https://doi.org/10.1134/S0020441221010280>
10. Mendes JC, Liehr M, Li C (2022) Diamond/GaN HEMTs: where from and where to? *Materials*. <https://doi.org/10.3390/ma15020415>
11. Mandal S (2021) Nucleation of diamond films on heterogeneous substrates: a review. *RSC Adv* 11(17):10159–10182. <https://doi.org/10.1039/d1ra00397f>
12. Zhu W, Yang PC, Glass JT (1993) Oriented diamond films grown on nickel substrates. *Appl Phys Lett* 63(12):1640–1642. <https://doi.org/10.1063/1.110721>
13. Moore E, Jarrell J, Cao L (2017) Heteroepitaxial diamond growth on 4H-SiC using microwave plasma chemical vapor deposition. *Heliyon* 3(9):e00404. <https://doi.org/10.1016/j.heliyon.2017.e00404>
14. Yang PC, Schlessler R, Wolden CA, Liu W, Davis RF, Sitar Z (1997) Control of diamond heteroepitaxy on nickel by optical reflectance. *Appl Phys Lett* 70(22):2960–2962. <https://doi.org/10.1063/1.118756>
15. Sato Y, Fujita H, Ando T, Tanaka T, Kamo M (1993) Local epitaxial growth of diamond on nickel from the vapour phase. *Philos Trans R Soc Lond Ser Phys Eng Sci* 342(1664):225–231. <https://doi.org/10.1098/rsta.1993.0016>
16. Hassan AW, Noordin MY, Izman S, Denni K, Nazim EM (2019) Modification of an electroplated nickel interlayer surface by annealing heat treatment for diamond deposition on tungsten carbide. *Metallogr Microstruct Anal* 8(2):201–211. <https://doi.org/10.1007/s13632-018-0512-8>
17. Lindroos J, Fenning DP, Backlund DJ, Verlage E, Gorgulla A, Estreicher SK, Savin H, Buonassisi T (2013) Nickel: a very fast diffuser in silicon. *J Appl Phys*. <https://doi.org/10.1063/1.4807799>
18. Guo X, Yu H, Jiang YL, Ru GP, Zhang DW, Li BZ (2011) Study of nickel silicide formation on Si(1 1 0) substrate. *Appl Surf Sci* 257(24):10571–10575. <https://doi.org/10.1016/j.apsusc.2011.07.052>
19. Chen LJ (2009) Silicide technology for integrated circuits, London: the institute of Engineering and Technology, London, United Kingdom, pp 95–143
20. Dutra AT, Ferrandini PL, Costa CAR, Gonçalves MC, Caram R (2005) Growth and solid/solid transformation in a Ni-Si eutectic alloy. *J Alloys Compd* 399(1–2):202–207. <https://doi.org/10.1016/j.jallcom.2005.03.039>
21. Koos V, Beck U, Neumann H-G (1976) Structure and intrinsic stress of nickel silicide films. *Phys Status Solidi A* 37(1):193–198. <https://doi.org/10.1002/pssa.2210370125>
22. Baker IAN, Yuan JUN, Schulson EM (1993) Formation of L12-structured Ni₃Si. *Metall Trans A* 24(February):283–292
23. Connétable D, Thomas O (2011) First-principles study of nickel-silicides ordered phases. *J Alloys Compd* 509(6):2639–2644. <https://doi.org/10.1016/j.jallcom.2010.10.118>
24. Ahmed R, Nazari M, Hancock BL, Simpson J, Engdahl C, Piner EL, Holtz MW (2018) Ultraviolet micro-Raman stress map of

- polycrystalline diamond grown selectively on silicon substrates using chemical vapor deposition. *Appl Phys Lett*. <https://doi.org/10.1063/1.5027507>
25. Lu HC, Peng YC, Lin MY, Chou SL, Lo JI, Cheng BM (2015) Analysis of nickel defect in diamond with photoluminescence upon excitation near 200 nm. *Anal Chem* 87(14):7340–7344. <https://doi.org/10.1021/acs.analchem.5b01493>
 26. Rey S, Hommet J, Schmerber G, Le Normand F (2000) Diamond growth on polycrystalline nickel silicides. *J Cryst Growth* 216(1):225–234. [https://doi.org/10.1016/S0022-0248\(00\)00365-1](https://doi.org/10.1016/S0022-0248(00)00365-1)
 27. Zhang WB, Chen C, Zhang SY (2013) Equilibrium crystal shape of Ni from first principles. *J Phys Chem C* 117(41):21274–21280. <https://doi.org/10.1021/jp404569m>
 28. Han L, Jeurgens LPH, Cancellieri C, Wang J, Xu Y, Huang Y, Liu Y, Wang Z (2020) Anomalous texture development induced by grain yielding anisotropy in Ni and Ni-Mo alloys. *Acta Mater* 200:857–868. <https://doi.org/10.1016/j.actamat.2020.09.063>
 29. Saha P, Nam C, Hickner MA, Zenyuk IV (2019) Electrokinetic streaming-current methods to probe the electrode-electrolyte interface under applied potentials. *J Phys Chem C* 123(32):19493–19505. <https://doi.org/10.1021/acs.jpcc.9b03430>
 30. Heyn E (1903) Short reports from the metallurgical and metallographic laboratory of the royal mechanical and technical testing institute of Charlottenburg. *The Metallographist* VI, pp 39–64
 31. Liu T, Raabe D, Mao WM (2010) A review of crystallographic textures in chemical vapor-deposited diamond films. *Front Mater Sci China* 4(1):1–16. <https://doi.org/10.1007/s11760-008-0099-7>
 32. Liu XZ, Wei QP, Zhai H, Yu ZM (2013) Enhancement of nucleation of diamond films deposited on copper substrate by nickel modification layer. *Trans Nonferrous Met Soc China Engl Ed* 23(3):667–673. [https://doi.org/10.1016/S1003-6326\(13\)62514-5](https://doi.org/10.1016/S1003-6326(13)62514-5)
 33. Kwong WY, Zhang WY (2005) Electron-beam assisted platinum deposition as a protective layer for FIB and TEM applications. *IEEE Int Symp Semicond Manuf Conf Proc*. <https://doi.org/10.1109/issm.2005.1513408>
 34. K.C. A, Saha R, Anderson J, Ayala A, Engdahl C, Piner EL, Holtz MW (2021) Effect of seeding density on the growth of diamond films by hot-filament chemical vapor deposition from sparse to dense range. *J Appl Phys*. <https://doi.org/10.1063/5.0068541>
 35. AKC (2022) Diamond Seeding Process for the Heterogenous Integration of High-Quality Diamond on Semiconductors," PhD Dissertation, Texas State University. [Online]. Available: <https://digital.library.txstate.edu/handle/10877/15661>
 36. Das D, Singh RN (2007) A review of nucleation, growth and low temperature synthesis of diamond thin films. *Int Mater Rev* 52(1):29–64. <https://doi.org/10.1179/174328007X160245>
 37. Guo Q, Guo Z, Shi J, Sang L, Gao B, Chen Q, Liu Z, Wang X (2018) Fabrication of nickel and nickel carbide thin films by pulsed chemical vapor deposition. *MRS Commun* 8(1):88–94. <https://doi.org/10.1557/mrc.2018.21>
 38. Zhang F, Song Z, Li J, Chen G (1991) Structure studies of synthetic diamond thin films by x-ray diffraction. *Thin Solid Films* 199(1):123–128. [https://doi.org/10.1016/0040-6090\(91\)90058-6](https://doi.org/10.1016/0040-6090(91)90058-6)
 39. Xi YF, Huang J, Tang K, Zhou XY, Ren B, Wang LJ (2018) Growth of highly (110) oriented diamond film by microwave plasma chemical vapor deposition. *Solid State Phenom* 281(110):893–899. <https://doi.org/10.4028/www.scientific.net/SSP.281.893>
 40. Chen Q, Wang L, Zhang Z, Yang J, Lin Z (1997) Epitaxially oriented growth of diamond on silicon by hot filament chemical vapor deposition Epitaxially oriented growth of diamond on silicon by hot filament chemical vapor deposition. *Appl Phys Lett* 176(1996):19–22. <https://doi.org/10.1063/1.116451>
 41. Kuang X, Tian J, Guo H, Hou Y, Zhang H, Liu T (2018) Feasible method to fabricate a nickel-nanodot mask on a silicon substrate with conventional thermal annealing. *Mater Technol* 52(2):119–123. <https://doi.org/10.17222/mit.2017.006>

Publisher's Note Springer Nature remains neutral with regard to jurisdictional claims in published maps and institutional affiliations.